Dual-output inverter with phase correction ability for dynamic WPT track supply

Hemant Dashora, Manuele Bertoluzzo*, and Giuseppe Buja, *Life Fellow, IEEE*
Department of Industrial Engineering, University of Padova, Padova, Italy
*Corresponding author: manuele.bertoluzzo@unipd.it

***Abstract* – Dynamic WPT systems are extensively investigated as a promising solution to the issues of the comparatively short range and long recharge time of the electric vehicles. In dynamic WPT systems, the lumped tracks exhibit greater power transfer efficiency than the stretched ones but require the supply of a large number of transmitting coils. This paper proposes a command strategy for a dual-output inverter that allows the concurrent supply of two track coils, with the ability of adjusting independently the voltage applied to each of them without altering the phase relation between the two supply currents. Moreover, if the series resonant compensation is used at the track side, the proposed strategy is robust against the onset of a reactive component in the loads seen at the inverter outputs as it inherently corrects the phase of the coil currents without making recourse to any additional control algorithm.**

Index Terms— Dynamic wireless charging, Track coil supply, Dual-output inverter.

I. INTRODUCTION

Despite their undoubted environmental sustainability, electric vehicles (EVs) are still struggling to become the first choice for a driver because of their short range, long recharge time and high cost, mainly due to the usage of batteries as on-board storage means. The dynamic wireless power transfer (DWPT) systems [1]-[3] are a promising solution to these issues because they offer the possibility of transferring electric power to a moving EV, thus making its range independent from the battery capacity and relieving the driver from the need of stopping to recharge the battery.

Track layout of the DWPT systems can be lumped or stretched. Lumped tracks enjoy a coupling coefficient that is on average higher than the stretched tracks, so that they transfer the power with greater efficiency. On the other hand, lumped tracks require the deployment of a multi-inverter supply infrastructure to power the track coils. An arrangement proposed to reduce the supply infrastructure consists in connecting more track coils to one inverter through switches that are closed according to the coil to be powered [4], [5].

Besides delivering the power, the supply infrastructure is also committed to execute coordination and synchronization tasks, f.i. to guarantee that two track coils coupled with the same pickup cooperate to the power transfer. This entails that the currents flowing into the two track coils must be in phase so that the magnetic fluxes produced by the track coils and linked with the pickup sum and produce a higher induced voltage.

Synchronization of the output currents of two inverters managed by independent controllers needs an exchange of phase-related information between the controllers, thus increasing the complexity of the supply infrastructure. Some solutions circumvent the information exchange by making recourse to a power stage with two or more inverters managed by a single controller [6]. In this case, there is the requirement of keeping at a minimum the complexity of the power stage in order to reduce the overall cost of the DWPT systems.

This paper proposes the use of a three-legs H-bridge to setup a dual-output inverter for the simultaneous supply of two track coils [7] and presents a dual-output command (DOC) strategy that allows the independent adjustment of the magnitude of the two generated voltages while maintaining the correct phase relation between the coil currents. Moreover, the paper demonstrates that, with track coils compensated for by series resonant capacitors, the DOC strategy exhibits an inherent robustness against the onset of a reactive component in the loads seen at the inverter outputs, hereafter shortly termed as the inverter loads. This reduces the phase error between the two track currents, compared to the case that their supply voltages are adjusted with the popular phase shift technique (PST).

The paper is organized as follows. Section II describes the power stage of the dual-output inverter and reviews functioning and limitations of the PST [8], [9]. Section III introduces the DOC strategy and describes its operation with resistive inverter loads. Section IV deals with the effects on the magnitude and the phase of the supply voltages of a reactive component in the inverter loads. Section V explains and quantifies the phase self-correction ability of the DOC strategy. Section VI reports the results of some tests carried out on the DOC strategy by simulation. Section VII concludes the paper.

II. PHASE SHIFT TECHNIQUE

The lumped track of a DWPT system is formed by a string of transmitting coils that, one after the other, are coupled with the pickup along the EV route, as sketched in Fig. 1. Depending on the distance D between two track coils, the pickup could be coupled simultaneously with two of them [3]. In this case, both track coils, denoted as Track Coil a (TCa) and Track Coil b (TCb) in Fig. 1, contribute to the power transfer, which is

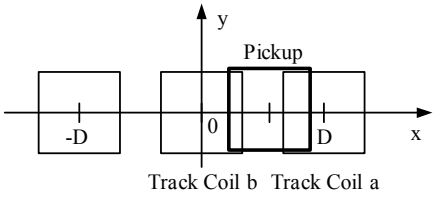

Fig.1. Layout of the track.

maximum when the currents flowing in the coils are in phase. This condition must be maintained irrespectively from the current magnitudes, which could differ according to the power demand of the EV, and from the inverter loads, which are affected, for example, by the variation of the track coil self-inductances caused by the change of the pickup core position with respect to them.

The DOC strategy for a dual-output inverter is developed under the assumptions that i) the track coils are compensated for by a series resonant capacitor, and ii) the same compensation is implemented in the pickup; in spite of its simplicity, the series-series compensation is very effective in limiting the inverter sizing power and in increasing the power transfer efficiency [10].

The standard solution to supply a single coil is shown in Fig. 2. The supply voltage v_{AC} is generated by a two-leg H-bridge that behaves as a single-phase inverter [11], [12]. The capacitor C_a resonates with the coil inductance L_a so that the inverter load is constituted only by the reflected impedance of the pickup; because of the series resonance also at the pickup side, it is purely resistive and is denoted with $R_{a,ref}$ in the figure.

The resonance forces the current to flow for the full supply period in both track coils and pickup, and to have a nearly sinusoidal waveform. As a consequence, only the first harmonic component of the inverter output voltage, denoted as $v_{AC,1}$, is involved in the power transfer. The magnitude I_a of the TCa current is regulated by adjusting the magnitude $V_{AC,1}$ of $v_{AC,1}$; this is done by help of the PST since the use of any PWM technique is prevented by the very high switching frequency of the inverter (commonly fixed at tens of kHz). The PST provides the gate commands to the legs LGa and LGc of the inverter with a 50% duty-cycle and a shift angle $\alpha_{a,ps}$ to set the voltage magnitude, where $\alpha_{a,ps}$ ranges from 0 to π. By disregarding the dead times, at any instant one of the power switches is on in both LGa and LGc so that the voltages v_{AO} and v_{CO} of the points A and C with respect to the virtual middle point O of the DC bus are imposed throughout the entire supply period. The waveform of v_{CO} is represented by the magenta dashed line in the upper half of Fig. 3 whilst that one of v_{AO} is represented by the red solid line. The waveforms have been drawn by assigning values a little different from 1 to the V_{DC}-normalized amplitudes so as to distinguish them. The supply voltage v_{AC} has the three-level waveform plotted with the red line in the lower half of Fig. 3.

The magnitude and the phase of $v_{AC,1}$ are worked out by expressing v_{AC} as a Fourier series in the form

$$v_{AC} = \sum_{n=1}^{\infty} s_n \sin(n\theta - \theta_n) \qquad (1)$$

Here and later the falling edge of v_{CO} is selected as the angular reference. This selection has the advantage that the (initial) phase

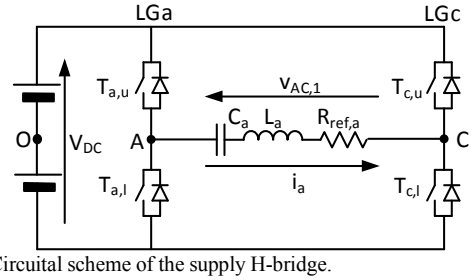

Fig. 2. Circuital scheme of the supply H-bridge.

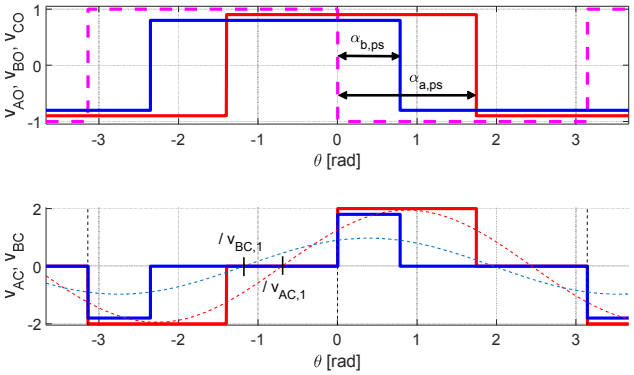

Fig. 3. Voltage waveforms generated by PST.

θ_1 of $v_{AC,1}$ corresponds to the positive zero crossing of $v_{AC,1}$ and that the comparison of expressions and plots of the subsequent waveforms processed throughout the paper is made easier.

Further to (1), the magnitude and the phase of $v_{AC,1}$ are given by

$$V_{AC,1} \triangleq s_1 = V_{dc}\frac{4}{\pi}sin\left(\frac{\alpha_{a,ps}}{2}\right) \qquad (2)$$

$$\angle v_{AC,1} \triangleq \theta_1 = -\frac{\pi}{2} + \frac{\alpha_{a,ps}}{2} \qquad (3)$$

By (2) and (3), voltage $v_{AC,1}$ has the waveform plotted with the red dashed line in the lower part of Fig. 3.

Simultaneous supply of TCa and TCb can be achieved using a three-leg H-bridge and connecting the coils as in Fig. 4. Such an arrangement is less expensive than the use of two separate inverters but requires sizing of LGc for the sum i_c of the currents i_a and i_b flowing in the two coils.

The magnitudes $V_{AC,1}$ and $V_{BC,1}$ are regulated independently in the range from 0 to $4/\pi V_{DC}$ by adjusting $\alpha_{a,ps}$ and $\alpha_{b,ps}$ according to (2). From (3), a difference in the shift angles affects the phase between the first harmonic components of the two output voltages, which can be expressed as

$$\angle(v_{AC,1}, v_{BC,1}) \triangleq \angle v_{AC,1} - \angle v_{BC,1} = \frac{\alpha_{a,ps}-\alpha_{b,ps}}{2} \qquad (4)$$

Eq. (4) is confirmed by the waveforms of Fig. 3, where v_{BO}, v_{BC} and $v_{BC,1}$ are plotted using the blue lines.

Being the inverter load purely resistive, the phase relation in (4) holds also for i_a and i_b; as explained above, a phase displacement between the two currents, like that one of the supply voltages in (4), impairs the power transfer capability of

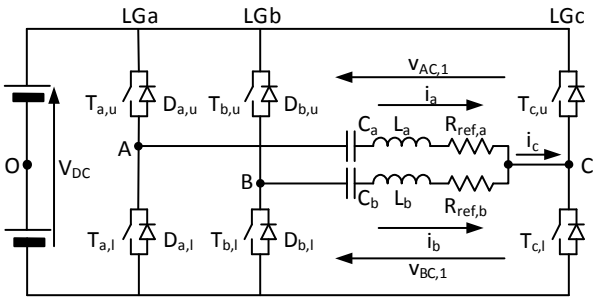

Fig. 4. Connection of a three-leg H-bridge to two track coils.

the DWPT system.

III. THE DOC STRATEGY

The DOC strategy is tailored to the circuit of Fig. 4 and is aimed at adjusting the two magnitudes $V_{AC,1}$ and $V_{BC,1}$ independently, while maintaining the currents i_a and i_b in phase, by imposing that

$$\angle(v_{AC,1}, v_{BC,1}) = 0 \tag{5}$$

With the DOC strategy, the switches of LGc are commanded as with the PST by gate signals having duty-cycle of 50% so that v_{CO} is imposed during the full supply period. Unlike the PST, the DOC strategy closes the upper switch $T_{a,u}$ of LGa only for an interval centered around $\pi/2$ and spanning α_a radians, and the lower switch $T_{a,l}$ of the same leg for an equal interval centered around $-\pi/2$; the same strategy is used for the command of the switches of LGb, the difference being that here the spanning angle is α_b. As a consequence, it exists a fraction of the supply period during which both switches of LGa and LGb are open and the amplitudes of v_{AO} and v_{BO} depend on whether the free-wheeling diodes are conducting or not. An example of waveforms of the voltages v_{AO}, v_{BO} and v_{CO} are plotted in the upper half of Fig. 5, using the same color codes as in Fig. 3 and highlighting by thick segments the intervals where one of the two switches of a leg is closed.

In agreement with the conventions of Fig. 4, when both switches of a leg are open, positive currents force the conduction of the lower diodes while negative currents forces that one of the upper diodes. With resistive inverter loads, the currents i_a and i_b are in phase to $v_{AC,1}$ and $v_{BC,1}$, as plotted in the upper half of Fig. 5, where both currents are represented with the dashed green line in an arbitrary scale. In the figure, the waveforms of v_{AO} and v_{CO} are completed with the dashed lines in correspondence to the diode conduction, and the conducting devices of LGa are indicated for each interval. The resulting voltages v_{AC} and v_{BC} are plotted in the lower half of Fig. 5. Their waveforms are equal to those generated with the PST, but are symmetrical with respect to $\theta = 0$. Hence, their first harmonic components have magnitude given by (2) and phase equal to

$$\angle v_{AC,1} = \angle v_{BC,1} = 0 \tag{6}$$

regardless of the values of α_a and α_b; this means that the condition (5) is verified for any pair of α_a and α_b.

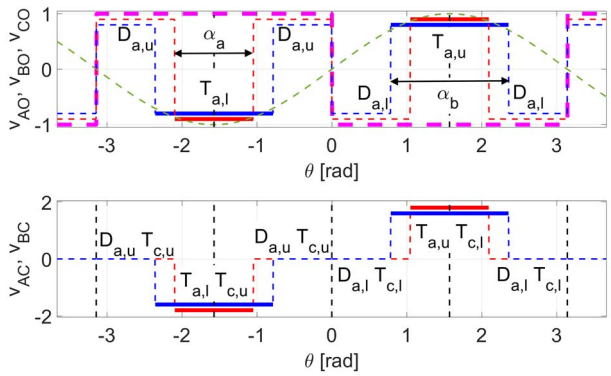

Fig. 5. Voltage waveforms generated by DOC strategy with $\angle i_a = 0$.

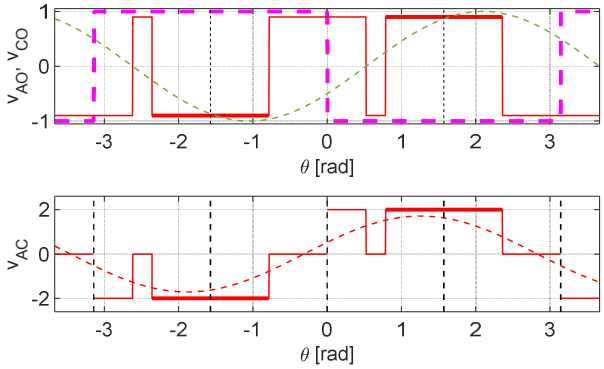

Fig. 6. Voltage waveforms generated by DOC strategy with $|\angle i_a| < (\pi/2 - \alpha_a/2)$.

IV. EFFECT OF LOAD REACTANCE

A variation of the self-inductances in any of the two track coils or in the pickup induces the onset of a reactive component in the inverter loads so that i_a and i_b are no more in phase to $v_{AC,1}$ and $v_{BC,1}$.

Let us consider the case that the onset of a reactive components occurs only on TCa so that the current i_a is out of phase to $v_{AC,1}$ while i_b is still in phase to $v_{BC,1}$. Depending on the value of $\angle i_a$, three different situations can be recognized that lead to as many expressions of $V_{AC,1}$ and $\angle v_{AC,1}$.

A. $|\angle i_a| < (\pi/2 - \alpha_a/2)$

At first, the operation of the circuit in Fig. 4 is analyzed when the phase of i_a is positive, i.e. $\angle i_a > 0$, and less than $(\pi/2 - \alpha_a/2)$. Differently from the situation illustrated in Section III, the diode $D_{a,u}$ is now kept in conduction after the falling edge of v_{CO} while the diode $D_{a,l}$ conducts even after the rising edge of v_{CO}, as plotted in the upper part of Fig. 6. The waveform of v_{AC} changes accordingly and is plotted in the lower part of the figure. The magnitude $V_{AC,1}$ increases since additional intervals arise where v_{AC} is different from zero, and the value of $\angle v_{AC,1}$ becomes negative since these intervals are placed on the left-hand side of the semi-periods of v_{CO}. Therefore, the positive zero crossing of $v_{AC,1}$ moves on the left and leads the falling edge of v_{CO}, as shown by the red dashed waveform in Fig. 6.

The expressions of $V_{AC,1}$ and $\angle v_{AC,1}$ change from (2) and (6) into

$$V_{AC,1} = V_{dc}\frac{2}{\pi}\sqrt{\left[1 - cos(\angle i_a) + 2sin\left(\frac{\alpha_a}{2}\right)\right]^2 + [sin(\angle i_a)]^2} \tag{7}$$

$$\angle v_{AC,1} = \text{atan}\left[-\frac{sin(\angle i_a)}{1 - cos(\angle i_a) + 2sin\left(\frac{\alpha_a}{2}\right)}\right] \tag{8}$$

It can be readily realized that, for $\angle i_a = 0$, expressions (7) and (8) simplify to (2) and (6). Moreover, it can be demonstrated that expressions (7) and (8) hold also for $-(\pi/2 - \alpha_a/2) < \angle i_a < 0$; in this case, the additional intervals where v_{AC} is different from zero are placed on the right side of the semi-periods of v_{CO} so that, according to (8), $\angle v_{AC,1}$ becomes positive.

B. $(\pi/2 - \alpha_a/2) < |\angle i_a| < (\pi/2 + \alpha_a/2)$

When the phase of i_a is positive and in-between $(\pi/2 - \alpha_a/2)$ and $(\pi/2 + \alpha_a/2)$, the waveforms of v_{AO} and v_{AC} change

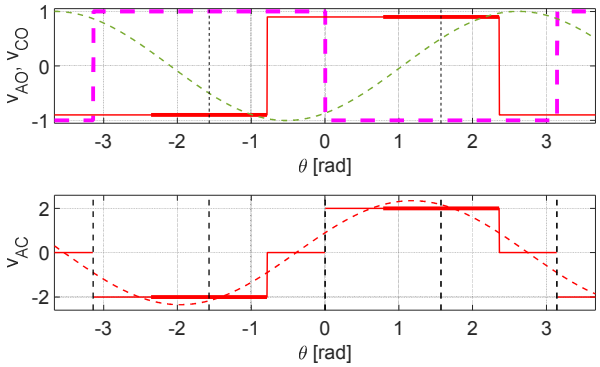

Fig. 7. Voltage waveforms generated by DOC strategy with $(\pi/2-\alpha_a/2) < |\angle i_a| < (\pi/2+\alpha_a/2)$.

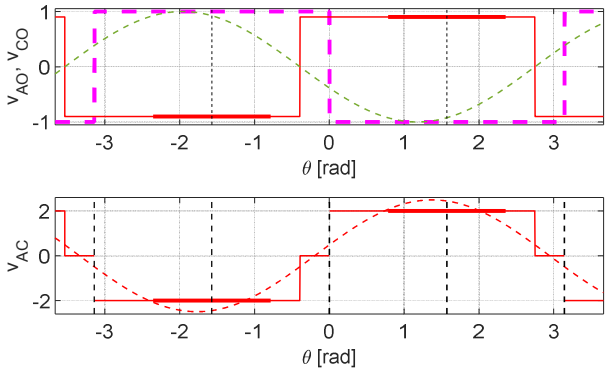

Fig. 8. Voltage waveforms generated by DOC strategy with $(\pi/2+\alpha_a/2) < |\angle i_a| < \pi$.

into those plotted in Fig. 7. During the positive semi-period of v_{CO}, the diode $D_{a,u}$ conducts until $T_{a,u}$ is switched on; consequently, voltage v_{AC} is positive in the full interval $0 < \theta < \pi/2 + \alpha_a/2$. During the negative semi-period of v_{CO}, voltage v_{AC} is negative in the interval $-\pi < \theta < -\pi/2 + \alpha_a/2$. Then, the waveform of v_{AC} is the same that would be generated by the PST with $\alpha_{a,ps} = \pi/2 + \alpha_a/2$; substitution of this angular value into (2) and (3) yields the following expressions of $V_{AC,1}$ and $\angle v_{AC,1}$:

$$V_{AC,1} = V_{dc}\frac{4}{\pi}sin\left(\frac{\pi/2+\alpha_a/2}{2}\right) \quad (9)$$

$$\angle v_{AC,1} = -\frac{\pi}{4} + \frac{\alpha_a}{4} \quad (10)$$

For $\angle i_a < 0$ and in-between $-(\pi/2+\alpha_a/2)$ and $-(\pi/2-\alpha_a/2)$, due to the symmetry of the waveform, $V_{AC,1}$ still takes the expression (9) while $\angle v_{AC,1}$ changes its sign, as occurred in (8), and its expression becomes

$$\angle v_{AC,1} = \frac{\pi}{4} - \frac{\alpha_a}{4} \quad (11)$$

It is worth to note that expressions (9)-(11) do not depend on the phase of i_a but only on α_a.

C. $(\pi/2+\alpha_a/2) < |\angle i_a| < \pi$

For $\angle i_a > 0$ and in-between $(\pi/2+\alpha_a/2)$ and π, the waveforms of v_{AO} and v_{AC} change into those plotted in Fig. 8. In this case, v_{AC} is positive in the full interval $0 < \theta < \angle i_a$ and its waveform is the same that would be generated by the PST with $\alpha_{a,ps} = \angle i_a$. Therefore, $V_{AC,1}$ and $\angle v_{AC,1}$ are now given by

$$V_{AC,1} = V_{dc}\frac{4}{\pi}sin\left(\frac{\angle i_a}{2}\right) \quad (12)$$

$$\angle v_{AC,1} = -\frac{\pi}{2} + \frac{\angle i_a}{2} \quad (13)$$

For $\angle i_a < 0$ and $\angle i_a$ in-between $-\pi$ and $-(\pi/2+\alpha_a/2)$, the expressions of $V_{AC,1}$ and $\angle v_{AC,1}$ can be derived from (12) and (13) by taking advantage of the symmetry of the waveforms, obtaining

$$V_{AC,1} = V_{dc}\frac{4}{\pi}sin\left(-\frac{\angle i_a}{2}\right) \quad (14)$$

$$\angle v_{AC,1} = \frac{\pi}{2} + \frac{\angle i_a}{2} \quad (15)$$

All the findings reported in the Subsections A, B and C hold also for $V_{BC,1}$ and $\angle v_{BC,1}$, when i_b is out of phase to $v_{BC,1}$.

V. Phase-Adjusting Property of the DOC Strategy

Eqs. (7), (8) and (12)-(15) use $\angle i_a$ as an independent variable to work out $\angle v_{AC,1}$. Actually, the reactive component of the inverter load affects directly $\angle(v_{AC,1}, i_a)$ while the value taken by $\angle i_a$ is consequential. The three quantities are related by

$$\angle(v_{AC,1}, i_a) \triangleq \angle v_{AC,1}(\alpha_a, \angle i_a) - \angle i_a \quad (16)$$

where the dependence of $\angle v_{AC,1}$ on α_a and $\angle i_a$ is highlighted.

By (16), the value of $\angle i_a$ can be found as a function of α_a, which is set by the inverter command, and the value of $\angle(v_{AC,1}, i_a)$, which is imposed by the inverter load. Phase $\angle i_a$ is computed numerically and is plotted in Fig. 9, where the curves relevant to three different values of α_a are plotted. Besides $\angle i_a$, the phase $-\angle(v_{AC,1}, i_a)$ is plotted with the dashed blue line to represent the situation of $\angle v_{AC,1}(\alpha_a, \angle i_a) = 0$ that, by (16), corresponds to the situation of $\angle i_a = -\angle(v_{AC,1}, i_a)$. To discuss all together the results obtained in Section IV, the curves have been drawn with $\angle(v_{AC,1}, i_a)$ spanning the interval $-\pi < \theta < \pi$ even if it can not exceed the interval $-\pi/2 < \theta < \pi/2$ otherwise the power would flow back from the pickup to the track coils.

Inspection of Fig. 9 shows that the inequality $|\angle i_a| < |\angle(v_{AC,1}, i_a)|$ holds for any value of α_a. This implies that, under the hypothesis of $\angle i_b = 0$, the phase difference $|\angle(i_a, i_b)|$ between the currents i_a and i_b is less affected by a reactive component of the inverter load than the phase $|\angle(v_{AC,1}, i_a)|$

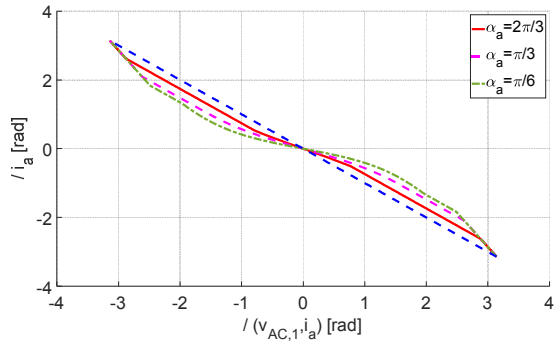

Fig. 9. $\angle i_a$ vs. $\angle(v_{AC,1}, i_a)$ for different values of α_a.

between the supply voltage and the current of TCa. The upshot can be explained by initially supposing that both inverter loads are resistive so that $\angle v_{AC,1} = \angle i_a = \angle i_b = 0$; then, by supposing that an inductance is inserted in series to $R_{a,ref}$. This insertion gives rise to a phase lag of i_a with respect to the initial situation, as shown in the upper half of Fig. 6; the phase lag, in turn, causes the appearance of the additional intervals mentioned in Section IV with v_{AC} different from zero and, consequently, the value of $\angle v_{AC,1}$ becomes negative, as shown in the lower half of Fig. 6. Being understood that the phase difference $\angle(v_{AC,1}, i_a)$ is related to the inverter load and, hence, is not influenced by the new value of $\angle v_{AC,1}$, the phase advance of $v_{AC,1}$ shifts i_a forward of an equal phase so that the resulting phase of i_a, is less than it would have been if $\angle v_{AC,1}$ had remained equal to zero, thus partially self-correcting the phase lag caused by the onset of the reactive component in the inverter load.

The self-correcting effect increases with $|\angle(v_{AC,1}, i_a)|$ as long as it is $|\angle i_a| < (\pi/2 - \alpha_a/2)$. Outside this interval, for $(\pi/2 - \alpha_a/2) < |\angle i_a| < (\pi/2 + \alpha_a/2)$, the value of $|\angle v_{AC,1}|$ does not decrease anymore and $|\angle(i_a, i_b)|$ starts increasing at the same rate of $|\angle(v_{AC,1}, i_a)|$, as per (10) and (11), even so $|\angle(i_a, i_b)|$ remains lower than $|\angle(v_{AC,1}, i_a)|$. Finally, for $(\pi/2 + \alpha_a/2) < |\angle i_a| < \pi$, the self-correcting effect continues, as per (13) and (15), but it becomes weaker and weaker as $|\angle(v_{AC,1}, i_a)|$ approximates π.

The DOC strategy discloses some self-correcting advantages also from the point of view of the magnitude of i_a. For a fixed magnitude $V_{AC,1}$, the onset of the reactive component in the inverter load would cause a decrease of I_a but, from (7), (9), (12) and (14), the magnitude $V_{AC,1}$ increases if $\angle i_a \neq 0$, thus contrasting this decrease. Fig. 10 plots $V_{AC,1}$ as a function of $\angle(v_{AC,1}, i_a)$ for the same values of α_a in Fig. 9. Like in the previous figure, three different situations can be recognized: for $|\angle i_a| < (\pi/2 - \alpha_a/2)$, the magnitude $V_{AC,1}$ increases more than proportionally to $|\angle(v_{AC,1}, i_a)|$; for $(\pi/2 - \alpha_a/2) < |\angle i_a| < (\pi/2 + \alpha_a/2)$, $V_{AC,1}$ is constant because, by (9), it is independent from $|\angle(v_{AC,1}, i_a)|$; finally, for $(\pi/2 + \alpha_a/2) < |\angle i_a| < \pi$, the magnitude $V_{AC,1}$ increases again by (12) and (14), and the three curves merge together, being $V_{AC,1}$ independent of α_a in this range of $|\angle i_a|$.

VI. Simulation Resuls

A number of simulations have been carried out in the Matlab-Simulink environment to substantiate the findings on the DOC strategy and to check if the phase difference $\angle(i_a, i_b)$ remains small enough not to impair the power transfer capability of the DWPT system under the possible variation of the self-inductance of the track coils due to the EV motion.

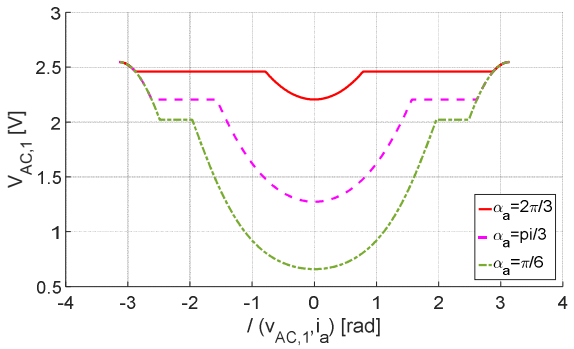

Fig. 10. $V_{AC,1}$ vs. $\angle(v_{AC,1}, i_a)$ for different values of α_a.

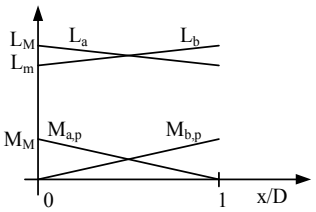

Fig.11. Self and mutual inductances vs. normalized pickup displacement.

A DWPT system with the coupling setup sketched in Fig. 1 is modeled. It is assumed that i) the track coils are deployed side by side so that there is no gap between their cores and the self-inductance of the pickup during its motion remains constant, and ii) the mutual inductance between the track coils is disregarded. With this track coil deployment, the mutual inductance $M_{a,p}$ between TCa and the pickup falls linearly from the maximum value M_M to zero while the pickup moves from the position of perfect alignment with TCa to that of perfect alignment with TCb; concurrently, the self-inductance L_a of the TCa decreases linearly from the maximum value L_M to the minimum value L_m, set 15% lower than L_M. The opposite occurs for the mutual inductance $M_{b,p}$ between TCb and the pickup, and for the self-inductance L_b of TCb. The profiles of the inductive quantities are plotted in Fig. 11 as a function of the displacement of the center of the pickup from that of TCa, normalized to the track coil distance D. The parameters of the DWPT system taken as a case study are listen in Tab. I; from them, it comes out that the resonant capacitors C_a and C_b are sized to resonate with L_M.

The dual-output inverter is commanded using the DOC strategy and the magnitudes of the currents i_a and i_b are kept constant by suitably modifying the angles α_a and α_b while the pickup moves from the position 0 to D. On account of the fact that the dynamics of the DWPT system are much faster those associated to the pickup motion, the system behavior is examined at ten discrete pickup positions equally spaced between 0 and D. As a comparison, the system behavior is also examined by commanding the dual-output inverter with the PST.

The waveforms of the currents i_a and i_b, and of their sum i_c at x/D equal to 0.1, 0.3 and 0.5 are plotted in Figs. 12, 13 and 14. Being L_a symmetric to L_b with respect to x/D=0.5 and $M_{a,p}$ symmetric to $M_{b,p}$ with respect to the same point, the waveforms relevant to the positions 0.9 and 0.7 are equal to those reported in the Figs. 12 and 13, provided that i_a and i_b exchange each other. The upper part of the figures plots the currents obtained with the DOC strategy, whilst the lower part refers to the PST. Comparison of the plots confirms that the DOC strategy

Table I. DWPT system parameters

Parameter	Symbol	Value
Track coil maximum self-inductance	L_M	120 µH
Resonant capacitors	C_a, C_b	29 nF
Maximum mutual inductance	M_M	30 µH
Supply angular frequency	ω	2π·85000 rad/s
Reflected loads	$R_{ref,a}$, $R_{ref,b}$	6.1 Ω
DC bus voltage	V_{DC}	350 V

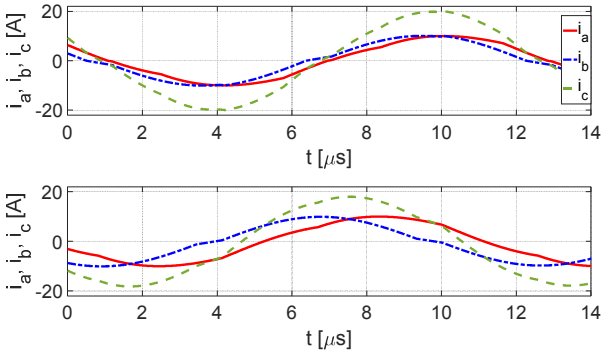

Fig. 12. Track coil currents i_a (red) and i_b (blue) and their sum (green) at normalized displacement = 0.1 generated by DOC strategy and PST.

maintains i_a and i_b nearly in phase despite the variation of the reactive components of the inverter loads. The PST does not perform equally well since a remarkable phase difference arises between i_a and i_b. At x/D=0.5, the pickup is exactly in the middle between TCa and TCb and the two track coils offer the same load impedance to the inverters; consequently, the waveform of i_a is equal to that of i_b for both the DOC strategy and the PST, as confirmed by Fig. 14.

Even if i_a and i_b reach the required magnitude at any pickup displacement with both supply approaches, the phase difference between the currents with the PST is such as to seriously affect the magnitude I_c of i_c, as shown in Fig. 15. Indeed, I_c is nearly constant with the pickup position with the DOC strategy whilst it decreases of more than 10% at x/D=0.2 and, by symmetry, at x/D=0.8 with the PST.

VII. Conclusions

The paper has proposed a dual-output command (DOC) strategy that allows the simultaneous supply of two track coils of a DWPT system with a three-leg H-bridge. The magnitudes of the voltages supplying the two coils can be adjusted independently while maintaining the coil currents in phase for resistive inverter loads and nearly in phase under the onset of a reactive component of the inverter loads. The strategy has been at first studied analytically and then substantiated by simulation. At last, it has been demonstrated that the performance of the DOC strategy outperform that of the PST significantly.

References

[1] R. Tavakoli and Z. Pantic, "Analysis, Design, and Demonstration of a 25-kW Dynamic Wireless Charging System for Roadway Electric Vehicles," *IEEE Journal of Emerging and Selected Topics in Power Electronics*, vol. 6, no. 3, pp. 1378-1393, Sept. 2018.

[2] H.K. Dashora, G. Buja, M. Bertoluzzo, R. Pinto, and V. Lopresto, "Analysis and design of DD coupler for dynamic wireless charging of electric vehicles," *Journal of Electromagnetic Waves and Applications*, vol. 32, no. 2, pp. 170-189, 2018.

[3] G. Buja, M. Bertoluzzo and H.K. Dashora, "Lumped Track Layout Design for Dynamic Wireless Charging of Electric Vehicles," *IEEE Transactions on Industrial Electronics*, vol. 63, no. 10, pp. 6631-6640, Oct. 2016.

[4] L. Shuguang, Y. Zhenxing and L. Wenbin, "Electric Vehicle Dynamic Wireless Charging Technology Based on Multi-parallel Primary Coils," in Proc, of 2018 IEEE Int. Conf. on Electronics and Communication Engineering (ICECE), 2018, pp. 120-124.

[5] H.K. Dashora, M. Bertoluzzo and G. Buja, "Reflexive properties for different pick-up circuit topologies in a distributed IPT track," in Proc. of IEEE Int. Conf. on Industrial Informatics (INDIN), 2015, pp. 69-75.

[6] C. Wang, C. Zhu, K. Song, G. Wei, S. Dong and R. G. Lu, "Primary-side control method in two-transmitter inductive wireless power transfer systems for dynamic wireless charging applications," in Proc. Of IEEE PELS Workshop on Emerging Technologies: Wireless Power Transfer (WoW), 2017, pp. 1-6.

[7] M. Bertoluzzo, G. Buja, and H. Dashora, "Avoiding Null Power Point in DD coils", in Proc. of IEEE PELS Workshop on Emerging Technologies: Wireless Power (WoW), 2019, pp. 1-6.

[8] D. Jang, "PWM methods for two-phase inverters," *IEEE Industry Applications Magazine*, vol. 13, no. 2, pp. 50-61, March-April 2007.

[9] C. Carretero, O. Lucía, J. Acero and J. M. Burdío, "Phase-shift control of dual half-bridge inverter feeding coupled loads for induction heating purposes," *Electronics Letters*, vol. 47, no. 11, pp. 670-671, May 2011.

[10] W. Zhang and C.C. Mi, "Compensation Topologies of High-Power Wireless Power Transfer Systems," *IEEE Transactions on Vehicular Technology*, vol. 65, no. 6, pp. 4768-4778, June 2016.

[11] M.H. Rashid, "Power Electronics circuits, devices, and applications," Third edition, Pearson/Prentice-Hall Publications, 2004.

[12] S. G. Rosu, M. Khalilian, V. Cirimele and P. Guglielmi, "A dynamic wireless charging system for electric vehicles based on DC/AC converters with SiC MOSFET-IGBT switches and resonant gate-drive," in Proc. of IEEE Industrial Electronics Society Ann. Conf. (IECON), 2016, pp. 4465-4470.

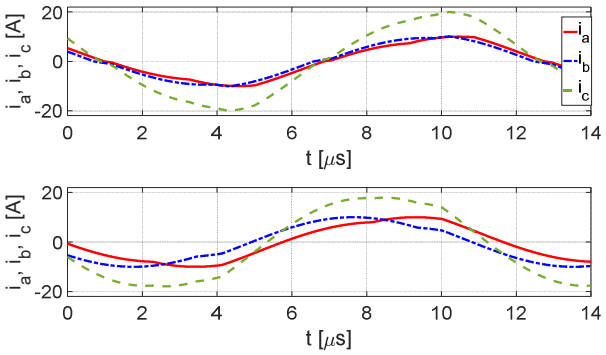

Fig. 13. Track coil currents i_a (red) and i_b (blue) and their sum (green) at normalized displacement = 0.3 for DOC strategy and PST.

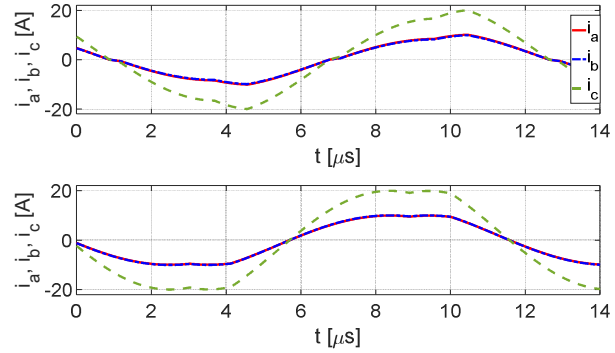

Fig. 14. Track coil currents i_a (red) and i_b (blue) and their sum (green) at normalized displacement = 0.5 generated by DOC strategy and PST.

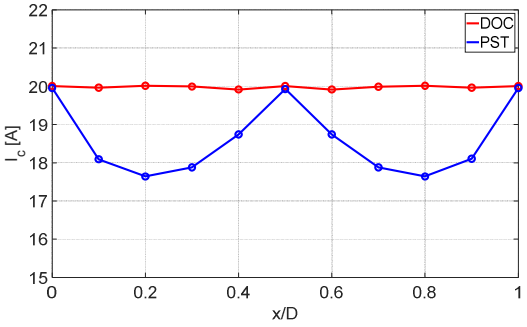

Fig. 15. Magnitude of i_c vs. normalized displacement.